J. Fluid Mech. (2006), *vol.* 555, *pp.* 43–58. © 2006 Cambridge University Press
doi:10.1017/S0022112006008664 Printed in the United Kingdom

Stability of the flow in a slowly diverging rectangular duct

By IOANNIS GALIONIS AND PHILIP HALL

Department of Mathematics, Imperial College, London SW7 2AZ, UK

(Received 1 November 2004 and in revised form 15 September 2005)

The spatial instability problem in a slowly diverging rectangular duct is investigated. The mean flow for the present problem is three-dimensional and has been obtained asymptotically using lubrication theory. Using a WKBJ expansion for the disturbance quantities, the zeroth- and first-order equations are derived. The zeroth-order problem corresponds to a locally parallel flow approximation and the first-order problem yields the non-parallel-flow correction to the eigenvalues obtained from the former through the use of a solvability condition. The solution of these equations is discussed and the results used to determine the effect of the variation in duct geometry on the neutral curves.

1. Introduction

Our concern is with the instability of flows which are locally unidirectional, but with the velocity field depending on the two variables normal to the flow direction and slowly on the variable in the flow direction. In aerodynamics, such flows are encountered in many situations, e.g. the corner flow near a wing–body junction and the flow over a short wing. In order to gain insight into the instability of this type of flow, here we consider another simpler flow that is common in engineering applications, i.e. the flow along a rectangular pipe. In most cases, the flow is turbulent and many studies have been performed in order to create a rigorous mathematical model to describe it based on empirical closure assumptions. The stability characteristics of this flow have been studied both experimentally and theoretically in the past and the results were either compared with or based on the plane Poiseuille flow between two parallel plates. Examples of the experimental studies include the works by Schiller (1923) and Davis & White (1928) who used a rectangular pipe of large aspect ratio. However, transition was estimated by the measurement of the head losses in the hydraulic experiments performed, and no controlled experimental results were produced. Furthermore, in the case of Davis & White, the estimated critical Reynolds numbers for various aspect ratios were unusually small. This was attributed to the nonlinear subcritical instability caused by the small depth of the experimental apparatus. In 1970, Kao & Park were able to perform experiments on a tube of 1:8 aspect ratio using artificial excitation produced by an oscillating ribbon and measuring the disturbances by means of hot-film anemometers. Measurements were taken for wavelengths, wave speeds and amplification rates. A critical Reynolds number was found at $Re_h = 2600$, where $Re_h = U_m d_h/\nu$ is the Reynolds number based on the hydraulic diameter $d_h = 4S/C$ (S being the aperture of the pipe and C the wetted perimeter) and the average flow velocity $U_m = Q/S$ (Q being the flow rate). Above this value of the Reynolds number,

https://doi.org/10.1017/S0022112006008664 Published online by Cambridge University Press

the breakdown of a growing wave occurred as a simultaneous increase of amplitude of various frequency modes and a decrease of the dominant mode amplitude.

The theoretical studies on this problem were hindered by numerical difficulties, since the flow is strictly two-dimensional and the computer resources were not sufficient at least until the early 1990s. Therefore, most of these studies correspond to the large-aspect-ratio limit and are based on the well-known behaviour of plane Poiseuille flow. As an example, the work by Hocking (1978) can be mentioned. He assumed that the instability remains similar to that of Poiseuille flow and the stability results for the rectangular pipe were taken to be perturbations of the unbounded solution. The 'central' region, where the flow resembles the Poiseuille flow, was considered separately from the regions close to the sidewalls. The results indicated an increase of the critical Reynolds number of $O(A^{-2})$, where A was the (large) aspect ratio of the pipe. The presence of a possible 'edge' mode located close to the sidewalls was not taken into account. In 1990, the report by Tatsumi & Yoshimura followed with numerical results for the stability of the complete rectangular pipe flow of arbitrary, but constant, aspect ratio. Their results showed the existence of four possible modes. At the limit of infinite aspect ratios (plane Poiseuille flow) two of these modes correspond to the symmetric $\tilde{v}$-disturbance which is known to be unstable at $Re = 5772$, whereas the other two correspond to the anti-symmetric $\tilde{v}$-disturbance which is stable. Results were taken for all the modes for $Re \leqslant 50\,000$ and it was concluded that the two modes that are stable for Poiseuille flow are stable for every value of A. The other two modes had increasing, but finite critical Reynolds numbers with decreasing aspect ratio. One of them was seen to have lower critical Reynolds numbers for all the aspect ratios (except at $A \to \infty$ where they become identical). However, no critical Reynolds number could be found for the most unstable mode for $A < 3.2$. Therefore, it was concluded that the flow is stable for $A < 3.2$. Finally, the presence of strong vortex layers was observed along the critical layer. The calculations of Tatsumi & Yoshimura (1990) were repeated by Theofilis, Duck & Owen (2004) who found good agreement with the previous work.

In the present report, we have focused on the most unstable mode of Tatsumi & Yoshimura (1990) and we have extended that work to the case of a rectangular pipe whose sidewalls are diverging slowly. This problem is related to the flow in a slowly diverging two-dimensional channel which has already been studied extensively using the lubrication theory. However, in this case, the laminar flow does not have a similarity solution and the mean flow has to be computed independently at each station. The presence of the crossflow velocity components leads to a system of three PDEs that depends on the rate of change of the aspect ratio and the local streamwise velocity component. The zeroth-order approximation to the linear stability problem corresponds to the case of constant-aspect-ratio pipe. The first-order system has a form similar to the zeroth-order, but with a non-zero right-hand side which depends on the crossflow velocities and the rate of change of A. It can be solved only when a solvability condition is satisfied. This condition provides the correction to the zeroth-order eigenvalue problem. The results indicate that there is a finite region of instability which depends on the Reynolds number and the streamwise velocity of the fluid at the entrance of the pipe.

The structure of the present paper is as follows. In § 2, the mean flow equations are derived. In § 3, the instability problem is formulated up to first-order terms consistent with the mean flow accuracy. In § 4, the results of both the mean flow and the instability problems are given. Finally, in § 5, some conclusions are drawn.

https://doi.org/10.1017/S0022112006008664 Published online by Cambridge University Press

2. The basic flow equations

Let the walls of the duct be defined by the following relations: $y = \pm 1$, $-A(\xi) \leqslant z \leqslant A(\xi)$ and $-1 \leqslant y \leqslant 1$, $z = \pm A(\xi)$. Here, we have defined $\xi = \epsilon x$. The incompressible non-dimensional Navier–Stokes equations describing the flow under study are:

continuity equation

$$\frac{\partial u}{\partial x} + \frac{\partial v}{\partial y} + \frac{\partial w}{\partial z} = 0, \tag{1}$$

x-momentum equation

$$\frac{\partial u}{\partial t} + u\frac{\partial u}{\partial x} + v\frac{\partial u}{\partial y} + w\frac{\partial u}{\partial z} = -\frac{\partial p}{\partial x} + \frac{1}{Re}\nabla^2 u, \tag{2}$$

y-momentum equation

$$\frac{\partial v}{\partial t} + u\frac{\partial v}{\partial x} + v\frac{\partial v}{\partial y} + w\frac{\partial v}{\partial z} = -\frac{\partial p}{\partial y} + \frac{1}{Re}\nabla^2 v, \tag{3}$$

z-momentum equation

$$\frac{\partial w}{\partial t} + u\frac{\partial w}{\partial x} + v\frac{\partial w}{\partial y} + w\frac{\partial w}{\partial z} = -\frac{\partial p}{\partial z} + \frac{1}{Re}\nabla^2 w. \tag{4}$$

In the above, ∇^2 is the Laplace operator in terms of the non-dimensional coordinates (x, y, z). Since we are interested in the steady mean flow problem, the unsteady terms will be dropped in what follows. Furthermore, since the duct is slowly divergent, the dependence of the flow quantities on the streamwise coordinate will be of the form $\boldsymbol{q} = \boldsymbol{q}(\epsilon x, y, z)$, where $\boldsymbol{q} = (u, v, w, p)^{tr}$ and $\epsilon \ll 1$ indicates the streamwise rate of change of the cross-sectional area. Moreover, this slow streamwise change indicates that the values of the normal and spanwise velocity components (v and w, respectively) will be a small perturbation to the solution corresponding to the duct with constant cross-sectional area, which is known to be identically zero. It will be shown that the pressure must have a dependence on the small parameter in order for its effects to remain in the equations. Since the downstream dependence of the flow is slow, we write

$$(u, v, w, p) = (\bar{u}, \epsilon\bar{v}, \epsilon\bar{w}, \epsilon^n(\bar{p}_0 + \epsilon^k \bar{p}_1)),$$

where n and k are constants to be found later and $\bar{u}$, $\bar{v}$, $\bar{w}$, $\bar{p}_0$ and $\bar{p}_1$ are of $O(1)$. Substituting in the continuity equation, we obtain:

$$\frac{\partial \bar{u}}{\partial \xi} + \frac{\partial \bar{v}}{\partial y} + \frac{\partial \bar{w}}{\partial z} = 0. \tag{5}$$

Furthermore, from the x-momentum equation, we find that diffusion balances the pressure gradient if $n = -1$, in which case we have:

$$\frac{\partial^2 \bar{u}}{\partial y^2} + \frac{\partial^2 \bar{u}}{\partial z^2} = Re\frac{\partial \bar{p}_0}{\partial \xi}. \tag{6}$$

Using the above value of n and taking $k = 2$ so that there is no pressure gradient accross the duct, we obtain for the y-momentum equation:

$$\frac{\partial \bar{p}_0}{\partial y} = 0, \quad \left(\frac{\partial^2 \bar{v}}{\partial y^2} + \frac{\partial^2 \bar{v}}{\partial z^2}\right) = Re\frac{\partial \bar{p}_1}{\partial y}, \tag{7a, b}$$

https://doi.org/10.1017/S0022112006008664 Published online by Cambridge University Press

Similarly for the z-momentum equation, we have:

$$\frac{\partial \bar{p}_0}{\partial z} = 0, \quad \left(\frac{\partial^2 \bar{w}}{\partial y^2} + \frac{\partial^2 \bar{w}}{\partial z^2}\right) = Re \frac{\partial \bar{p}_1}{\partial z}. \tag{8a, b}$$

The first of these two sets of equations indicates that the pressure at zeroth-order accuracy depends only on the streamwise direction, and the x-momentum equation can be written as:

$$\frac{\partial^2 \bar{u}}{\partial y^2} + \frac{\partial^2 \bar{u}}{\partial z^2} = Re \frac{\mathrm{d}\bar{p}_0}{\mathrm{d}\xi}. \tag{9}$$

The boundary conditions for this equation are the no-slip condition on the walls. However, the symmetry of the duct, and therefore of the basic flow, with respect to the axes $(y, 0)$ and $(0, z)$ can be used in order to study just a quarter of the domain; let us say the lower left-hand one. In this case, the boundary conditions for $\bar{u}$ become:

$$\left.\begin{array}{l} \text{lower and left-hand walls } (-1, z) \text{ and } (y, -A) : \bar{u} = 0, \\ \text{upper and right-hand (flow) boundaries } (0, z) \text{ and } (y, 0) : \dfrac{\partial \bar{u}}{\partial n} = 0, \end{array}\right\} \tag{10}$$

where n denotes the direction normal to each boundary. Using the linear dependence of $\bar{u}$ on the pressure gradient and the Reynolds number as indicated by equation (9), we can write the solution of this equation as follows:

$$\bar{u}(\xi, y, z) = \bar{\bar{u}}(\xi, y, z) Re \frac{\mathrm{d}\bar{p}_0}{\mathrm{d}\xi}, \tag{11}$$

where:

$$\frac{\partial^2 \bar{\bar{u}}}{\partial y^2} + \frac{\partial^2 \bar{\bar{u}}}{\partial z^2} = 1,$$

and $\bar{\bar{u}}$ is also a function of ξ since the boundaries' position changes with ξ. Following Rosenhead (1963) the solution of this equation can be written as follows:

$$\bar{\bar{u}}(\xi, y, z) = \frac{y^2 - 1}{2} + 2 \sum_{m=0}^{+\infty} \left[\frac{(-1)^m}{\lambda_m^3} \frac{\cosh(\lambda_m z)}{\cosh(\lambda_m A(\xi))} \cos(\lambda_m y) \right], \tag{12}$$

where $\lambda_m = (2m + 1)\pi/2$.

Now we return to the continuity equation. If we integrate equation (5) over the cross-section, we obtain:

$$\int_{-A(\xi)}^{A(\xi)} \int_{-1}^{1} \left(\frac{\partial \bar{u}}{\partial \xi} + \frac{\partial \bar{v}}{\partial y} + \frac{\partial \bar{w}}{\partial z}\right) \mathrm{d}y \, \mathrm{d}z = 0 \Rightarrow$$
$$\int_{-A(\xi)}^{A(\xi)} \int_{-1}^{1} \frac{\partial \bar{u}}{\partial \xi} \, \mathrm{d}y \, \mathrm{d}z + \int_{-A(\xi)}^{A(\xi)} [\bar{v}]_{-1}^{1} \, \mathrm{d}z + \int_{-1}^{1} [\bar{w}]_{-A(\xi)}^{A(\xi)} \, \mathrm{d}y = 0.$$

The last two integrals above are identically equal to zero because of the boundary conditions on the walls. Furthermore, the partial derivative with respect to ξ can be taken out of the first integral, again by using the boundary conditions on the walls. Therefore,

$$\frac{\mathrm{d}}{\mathrm{d}\xi} \left(\int_{-A(\xi)}^{A(\xi)} \int_{-1}^{1} \bar{u} \, \mathrm{d}y \, \mathrm{d}z \right) = 0. \tag{13}$$

https://doi.org/10.1017/S0022112006008664 Published online by Cambridge University Press

Finally, using equation (11), we obtain:

$$\frac{\mathrm{d}}{\mathrm{d}\xi}\left(\int_{-A(\xi)}^{A(\xi)}\int_{-1}^{1}\bar{\bar{u}}(\xi,y,z)\frac{\mathrm{d}\bar{p}_0}{\mathrm{d}\xi}\,\mathrm{d}y\,\mathrm{d}z\right)=0\Rightarrow$$

$$\frac{\mathrm{d}}{\mathrm{d}\xi}\left[\left(\int_{-A(\xi)}^{A(\xi)}\int_{-1}^{1}\bar{\bar{u}}(\xi,y,z)\,\mathrm{d}y\,\mathrm{d}z\right)\frac{\mathrm{d}\bar{p}_0}{\mathrm{d}\xi}\right]=0, \tag{14}$$

which is the Reynolds equation of lubrication theory and can be integrated once in order to yield:

$$\left.\frac{\mathrm{d}\bar{p}_0}{\mathrm{d}\xi}\right|_{\xi}=\frac{I(\xi_0)}{I(\xi)}\left.\frac{\mathrm{d}\bar{p}_0}{\mathrm{d}\xi}\right|_{\xi=\xi_0}, \tag{15}$$

where

$$I(\xi)=\int_{-A(\xi)}^{A(\xi)}\int_{-1}^{1}\bar{\bar{u}}(\xi,y,z)\,\mathrm{d}y\,\mathrm{d}z.$$

Using expression (12) it is possible to calculate this integral analytically and therefore specify the right-hand side of equation (11). Indeed,

$$I(\xi)=8\sum_{m=0}^{+\infty}\frac{\tanh(\lambda_m A)}{\lambda_m^5}-\frac{4A}{3}, \tag{16}$$

and the expression for $\bar{u}$ becomes:

$$\bar{u}(\xi,y,z)=\left(I(\xi_0)Re\left.\frac{\mathrm{d}\bar{p}_0}{\mathrm{d}\xi}\right|_{\xi=\xi_0}\right)\frac{\bar{\bar{u}}(\xi,y,z)}{I(\xi)}. \tag{17}$$

Without loss of generality, we can select the product of the Reynolds number and the initial pressure gradient to satisfy the relation:

$$Re\left.\frac{\mathrm{d}\bar{p}_0}{\mathrm{d}\xi}\right|_{\xi=\xi_0}\bar{\bar{u}}(\xi_0,0,0)=\kappa_0,$$

in which case, equation (17) becomes:

$$\bar{u}(\xi,y,z)=\kappa\frac{\bar{\bar{u}}(\xi,y,z)}{I(\xi)}, \tag{18}$$

with $\kappa=\kappa_0 I(\xi_0)/\bar{\bar{u}}(\xi_0,0,0)$, so that at $\xi=\xi_0$, the maximum value of $\bar{u}$ is κ_0.

On the other hand, equations (5), (7*b*) and (8*b*) form a system of equations that has to be solved simultaneously. However, this system will be manipulated even further in order to be solved efficiently. Towards this end, we cross-differentiate (7) and (8) and subtract one from the other. In this way the quantity

$$\theta=\frac{\partial\bar{v}}{\partial z}-\frac{\partial\bar{w}}{\partial y} \tag{19}$$

appears, which can be seen to be the vorticity function and it satisfies Laplace's equation: $\nabla^2\theta=0$. Furthermore, using the continuity equation (5) and the definition of vorticity we can derive two more equations:

$$\begin{aligned}\nabla^2\bar{v}-\frac{\partial\theta}{\partial z}&=-\frac{\partial^2\bar{u}}{\partial\xi\,\partial y},\\ \nabla^2\bar{w}+\frac{\partial\theta}{\partial y}&=-\frac{\partial^2\bar{u}}{\partial\xi\,\partial z}.\end{aligned} \tag{20}$$

https://doi.org/10.1017/S0022112006008664 Published online by Cambridge University Press

The right-hand side of these equations can be calculated using equations (12), (16) and (18).

The boundary conditions required to solve the above equations are as follows:

$$\left.\begin{aligned}
&\text{left-hand wall } (y,-A): \bar{v}=\bar{w}=\theta-\frac{\partial\bar{v}}{\partial z}=0,\\
&\text{right-hand (flow) boundary } (y,0): \frac{\partial\bar{v}}{\partial z}=\bar{w}=\theta=0,\\
&\text{lower wall } (-1,z): \bar{v}=\bar{w}=\theta+\frac{\partial\bar{w}}{\partial y}=0,\\
&\text{upper (flow) boundary } (z,0): \bar{v}=\frac{\partial\bar{w}}{\partial y}=\theta=0.
\end{aligned}\right\} \tag{21}$$

3. Linear stability equations

In order to derive the linear stability equations, we express the flow field as the superposition of the basic flow quantities with the corresponding perturbations that are assumed to be of very small size, so that their products and powers can be dropped:

$$\begin{aligned}
u&=\bar{u}+\hat{u},\\
v&=\epsilon\bar{v}+\hat{v},\\
w&=\epsilon\bar{w}+\hat{w},\\
p&=\epsilon^{-1}\bar{p}+\hat{p}.
\end{aligned}$$

The linearized disturbance equations take the form

$$\frac{\partial\hat{u}}{\partial x}+\frac{\partial\hat{v}}{\partial y}+\frac{\partial\hat{w}}{\partial z}=0, \tag{22}$$

$$\frac{\partial\hat{u}}{\partial t}+\bar{u}\frac{\partial\hat{u}}{\partial x}+\hat{u}\frac{\partial\bar{u}}{\partial x}+\hat{v}\frac{\partial\bar{u}}{\partial y}+\epsilon\bar{v}\frac{\partial\hat{u}}{\partial y}+\hat{w}\frac{\partial\bar{u}}{\partial z}+\epsilon\bar{w}\frac{\partial\hat{u}}{\partial z}=-\frac{\partial\hat{p}}{\partial x}+\frac{1}{Re}\left(\frac{\partial^2\hat{u}}{\partial x^2}+\frac{\partial^2\hat{u}}{\partial y^2}+\frac{\partial^2\hat{u}}{\partial z^2}\right), \tag{23}$$

$$\frac{\partial\hat{v}}{\partial t}+\bar{u}\frac{\partial\hat{v}}{\partial x}+\epsilon\hat{u}\frac{\partial\bar{v}}{\partial x}+\epsilon\hat{v}\frac{\partial\bar{v}}{\partial y}+\epsilon\bar{v}\frac{\partial\hat{v}}{\partial y}+\epsilon\hat{w}\frac{\partial\bar{v}}{\partial z}+\epsilon\bar{w}\frac{\partial\hat{v}}{\partial z}=-\frac{\partial\hat{p}}{\partial y}+\frac{1}{Re}\left(\frac{\partial^2\hat{v}}{\partial x^2}+\frac{\partial^2\hat{v}}{\partial y^2}+\frac{\partial^2\hat{v}}{\partial z^2}\right), \tag{24}$$

$$\begin{aligned}
\frac{\partial\hat{w}}{\partial t}+\bar{u}\frac{\partial\hat{w}}{\partial x}+\epsilon\hat{u}\frac{\partial\bar{w}}{\partial x}+\epsilon\hat{v}\frac{\partial\bar{w}}{\partial y}+\epsilon\bar{v}\frac{\partial\hat{w}}{\partial y}+\epsilon\hat{w}\frac{\partial\bar{w}}{\partial z}+\epsilon\bar{w}\frac{\partial\hat{w}}{\partial z}&\\
=-\frac{\partial\hat{p}}{\partial z}+\frac{1}{Re}\left(\frac{\partial^2\hat{w}}{\partial x^2}+\frac{\partial^2\hat{w}}{\partial y^2}+\frac{\partial^2\hat{w}}{\partial z^2}\right).&
\end{aligned} \tag{25}$$

Once again we let $\hat{\boldsymbol{q}}=(\hat{u},\hat{v},\hat{w},\hat{p})^{tr}$. Now we let $\hat{\boldsymbol{q}}(\xi,y,z,t)=\tilde{\boldsymbol{q}}(\xi,y,z)\exp(\int^{\xi}\epsilon^{-1}a(\xi_1)\,\mathrm{d}\xi_1-\mathrm{i}\omega t)$ where $\tilde{\boldsymbol{q}}(\xi,y,z)=\tilde{\boldsymbol{q}}_0(\xi,y,z)+\epsilon\tilde{\boldsymbol{q}}_1(\xi,y,z)$ and $a(\xi)=a_0(\xi)+\epsilon a_1(\xi)$. The zeroth- and first-order systems can be formulated as follows:

$$\text{zeroth order: } \mathscr{K}\tilde{q}_0=0, \tag{26}$$

$$\text{first order: } \quad \mathscr{K}\tilde{q}_1=f, \tag{27}$$

https://doi.org/10.1017/S0022112006008664 Published online by Cambridge University Press

where,

$$\mathscr{K} = \begin{bmatrix} a_0 & \dfrac{\partial}{\partial y} & \dfrac{\partial}{\partial z} & 0 \\ \mathrm{L} & \dfrac{\partial \bar{u}}{\partial y} & \dfrac{\partial \bar{u}}{\partial z} & a_0 \\ 0 & \mathrm{L} & 0 & \dfrac{\partial}{\partial y} \\ 0 & 0 & \mathrm{L} & \dfrac{\partial}{\partial z} \end{bmatrix},$$

$$\mathrm{L} = -Re^{-1}\left(a_0^2 + \frac{\partial^2}{\partial y^2} + \frac{\partial^2}{\partial z^2}\right) + a_0\bar{u} - \mathrm{i}\omega,$$

and $f = (f_1, f_2, f_3, f_4)^{tr}$, where,

$$f_1 = -a_1\tilde{u}_0 - \frac{\partial \tilde{u}_0}{\partial \xi}, \tag{28a}$$

$$f_2 = a_1\left[\left(\frac{2a_0}{Re} - \bar{u}\right)\tilde{u}_0 - \tilde{p}_0\right] + \left[\left(\frac{2a_0}{Re} - \bar{u}\right)\frac{\partial \tilde{u}_0}{\partial \xi} - \frac{\partial \tilde{p}_0}{\partial \xi} + \left(\frac{1}{Re}\frac{\mathrm{d}a_0}{\mathrm{d}\xi} - \frac{\partial \bar{u}}{\partial \xi}\right)\tilde{u}_0 - \bar{v}\frac{\partial \tilde{u}_0}{\partial y} - \bar{w}\frac{\partial \tilde{u}_0}{\partial z}\right], \tag{28b}$$

$$f_3 = a_1\left(\frac{2a_0}{Re} - \bar{u}\right)\tilde{v}_0 + \left[\left(\frac{2a_0}{Re} - \bar{u}\right)\frac{\partial \tilde{v}_0}{\partial \xi} + \left(\frac{1}{Re}\frac{\mathrm{d}a_0}{\mathrm{d}\xi} - \frac{\partial \bar{v}}{\partial y}\right)\tilde{v}_0 - \bar{v}\frac{\partial \tilde{v}_0}{\partial y} - \bar{w}\frac{\partial \tilde{v}_0}{\partial z} - \frac{\partial \bar{v}}{\partial z}\tilde{w}_0\right], \tag{28c}$$

$$f_4 = a_1\left(\frac{2a_0}{Re} - \bar{u}\right)\tilde{w}_0 + \left[\left(\frac{2a_0}{Re} - \bar{u}\right)\frac{\partial \tilde{w}_0}{\partial \xi} + \left(\frac{1}{Re}\frac{\mathrm{d}a_0}{\mathrm{d}\xi} - \frac{\partial \bar{w}}{\partial z}\right)\tilde{w}_0 - \frac{\partial \bar{w}}{\partial y}\tilde{v}_0 - \bar{v}\frac{\partial \tilde{w}_0}{\partial y} - \bar{w}\frac{\partial \tilde{w}_0}{\partial z}\right]. \tag{28d}$$

The zeroth-order problem is a quadratic eigenvalue problem, since the operator L includes the eigenvalue a_0 raised to the second power. Furthermore, the boundary conditions require that the disturbance velocity components vanish at the boundary. No boundary conditions need be specified for the pressure. A simplification could be made by taking into account the symmetry of the duct with respect to the planes xy and xz whose line of intersection coinsides with the $x = 0$ line. This symmetry would enable the appearance of four possible modes whose crossflows are shown in figure 1.

The boundary conditions for these modes valid for the lower left-hand quarter of the domain are $(\tilde{u}, \tilde{v}, \tilde{w}) = \mathbf{0}$ on the walls and as follows for the 'flow boundaries':

$$\left.\begin{array}{lllll} \text{Mode I:} & \text{Along } y = 0, z \in [-A(\xi), 0]: & \tilde{u} = 0, & \tilde{v}_y = 0, & \tilde{w} = 0, \\ & \text{Along } y \in [-1, 0], z = 0: & \tilde{u}_z = 0, & \tilde{v}_z = 0, & \tilde{w} = 0, \\ \text{Mode II:} & \text{Along } y = 0, z \in [-A(\xi), 0]: & \tilde{u} = 0, & \tilde{v}_y = 0, & \tilde{w} = 0, \\ & \text{Along } y \in [-1, 0], z = 0: & \tilde{u} = 0, & \tilde{v} = 0, & \tilde{w}_z = 0, \\ \text{Mode III:} & \text{Along } y = 0, z \in [-A(\xi), 0]: & \tilde{u}_y = 0, & \tilde{v} = 0, & \tilde{w}_y = 0, \\ & \text{Along } y \in [-1, 0], z = 0: & \tilde{u}_z = 0, & \tilde{v}_z = 0, & \tilde{w} = 0, \\ \text{Mode IV:} & \text{Along } y = 0, z \in [-A(\xi), 0]: & \tilde{u}_y = 0, & \tilde{v} = 0, & \tilde{w}_y = 0, \\ & \text{Along } y \in [-1, 0], z = 0: & \tilde{u} = 0, & \tilde{v} = 0, & \tilde{w}_z = 0. \end{array}\right\} \tag{29}$$

https://doi.org/10.1017/S0022112006008664 Published online by Cambridge University Press

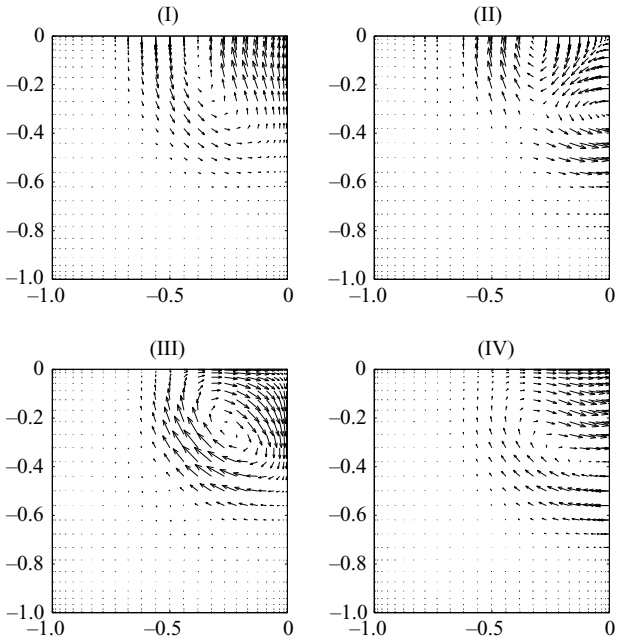


FIGURE 1. The crossflows corresponding to the four possible modes.

However, computationally we have used the shift-invert spectral transformation which requires the inversion of matrix $\mathscr{K}$ with $\alpha = \sigma$, where σ is the shift. Details of the method can be found in Saad (1992). Preliminary results showed that this would create a matrix for the solution of the eigenvalue problem with a very large condition number, something that would hinder convergence of the iterative solver used to 'invert' this matrix. Therefore, we have proceeded with the full problem and we have used the above symmetry properties in order to classify the resulting eigenvectors (disturbances). Full details of the numerical schemes and the checks made to verify the scheme can be found in Galionis (2003).

As far as the first-order problem is concerned, a solution is possible only when a solvability condition is satisfied. This can be formulated in the process using the adjoint problem, whose solution will be required for the solution of the solvability condition. After some calculations, the adjoint system can be formulated exactly like the zeroth-order problem ($\mathscr{K}_a Q = 0$), where

$$\mathscr{K}_a = \begin{bmatrix} a_0 & -\dfrac{\partial}{\partial y} & -\dfrac{\partial}{\partial z} & 0 \\ \mathrm{L} & 0 & 0 & a_0 \\ \dfrac{\partial \bar{u}}{\partial y} & \mathrm{L} & 0 & -\dfrac{\partial}{\partial y} \\ \dfrac{\partial \bar{u}}{\partial z} & 0 & \mathrm{L} & -\dfrac{\partial}{\partial z} \end{bmatrix}.$$

The operator L and the boundary conditions are the same as the zeroth-order problem. Finally, the solvability condition has the form:

$$\iint_{\Omega} (f_1 P + f_2 U + f_3 V + f_4 W)\, \mathrm{d}\Omega = 0. \tag{30}$$

https://doi.org/10.1017/S0022112006008664 Published online by Cambridge University Press

As can be seen from (28), each of the terms f_i can be split into two parts, the first of which is proportional to a_1. Therefore, if we write $f_i = a_1 f_{i1} - f_{i2}$, $i = 1, 2, 3, 4$, we can obtain:

$$a_1 \int\int_{\Omega} (f_{11}P + f_{21}U + f_{31}V + f_{41}W)\,\mathrm{d}\Omega = \int\int_{\Omega} (f_{12}P + f_{22}U + f_{32}V + f_{42}W)\,\mathrm{d}\Omega, \quad (31)$$

which can be solved for a_1. This quantity can be subsequently used in order to calculate the position of the neutral curve of the actual non-parallel flow. In particular, suppose we define the neutral curve by $\mathrm{Re}\{a(\xi_n)\} = 0$. To zeroth order in ϵ the growth rate at a point in the flow is unique, but at order ϵ it will depend on the flow quantity used and the position in the flow where it is sampled: see for example Gaster (1974). Thus, if we define the neutral curve by $\mathrm{Re}\{a(\xi_n)\} = 0$, then we are neglecting the rate of change of the disturbance quantities with respect to ξ. In fact, to the graphical accuracy of the results presented here, the latter effect is negligible. Expanding $\mathrm{Re}\{a(\xi)\}$ in a Taylor series around the position ξ_0 corresponding to the neutral curve of the parallel-flow approximation, we obtain:

$$\begin{aligned}\mathrm{Re}\{a(\xi_n)\} = 0 &= \mathrm{Re}\{a_0(\xi_n)\} + \epsilon\mathrm{Re}\{a_1(\xi_n)\} \\ &\approx \epsilon\mathrm{Re}\{a_1(\xi_0)\} + \mathrm{Re}\{a_0'(\xi_0)\}\delta\xi + \tfrac{1}{2}\mathrm{Re}\{a_0''(\xi_0)\}\delta\xi^2.\end{aligned}$$

This is a quadratic equation in $\delta\xi$ with solutions:

$$\delta\xi_{1,2} = \frac{\mathrm{Re}\{a_0'(\xi_0)\}}{-\mathrm{Re}\{a_0''(\xi_0)\}} \pm \sqrt{\left(\frac{\mathrm{Re}\{a_0'(\xi_0)\}}{-\mathrm{Re}\{a_0''(\xi_0)\}}\right)^2 + \frac{2\epsilon\mathrm{Re}\{a_1(\xi_0)\}}{-\mathrm{Re}\{a_0''(\xi_0)\}}}.$$

Although the second term inside the square root contains the small parameter ϵ, in the general case, we cannot simplify this expression further, because the two terms in the square root can be of the same order in the vicinity of the region where the upper and lower branches of the parallel-flow neutral curve approach each other. Taking into account that $-\mathrm{Re}\{a_0''(\xi_0)\} > 0$ along the neutral curve, we can select the proper sign in the above expression for $\delta\xi$ based on the sign of $\mathrm{Re}\{a_0'(\xi_0)\}$. Indeed,

$$\delta\xi = \begin{cases} \dfrac{\mathrm{Re}\{a_0'(\xi_0)\}}{-\mathrm{Re}\{a_0''(\xi_0)\}} - \sqrt{\left(\dfrac{\mathrm{Re}\{a_0'(\xi_0)\}}{-\mathrm{Re}\{a_0''(\xi_0)\}}\right)^2 + \dfrac{2\epsilon\mathrm{Re}\{a_1(\xi_0)\}}{-\mathrm{Re}\{a_0''(\xi_0)\}}} & \text{when } \mathrm{Re}\{a_0'(\xi_0)\} > 0. \\ \dfrac{\mathrm{Re}\{a_0'(\xi_0)\}}{-\mathrm{Re}\{a_0''(\xi_0)\}} + \sqrt{\left(\dfrac{\mathrm{Re}\{a_0'(\xi_0)\}}{-\mathrm{Re}\{a_0''(\xi_0)\}}\right)^2 + \dfrac{2\epsilon\mathrm{Re}\{a_1(\xi_0)\}}{-\mathrm{Re}\{a_0''(\xi_0)\}}} & \text{when } \mathrm{Re}\{a_0'(\xi_0)\} < 0. \end{cases} \quad (32)$$

Here, the derivatives must be evaluated numerically after a_0, a_1 have been calculated. Note again that the above correction of the position of the neutral curve was based on the assumption that the first-order term in the expansion of the growth rate a_1 is the only term that plays a role in the 'description' of the non-parallel effects. We have ignored this contribution, since, as stated above, to graphical accuracy, a_1 gives a satisfactory indication of the actual position of the non-parallel neutral curve. We note also that if, for example, we follow Hall (1983) and define the local growth rate on the disturbance energy integrated accross a cross-section, then we find that the results presented below are unchanged.

https://doi.org/10.1017/S0022112006008664 Published online by Cambridge University Press

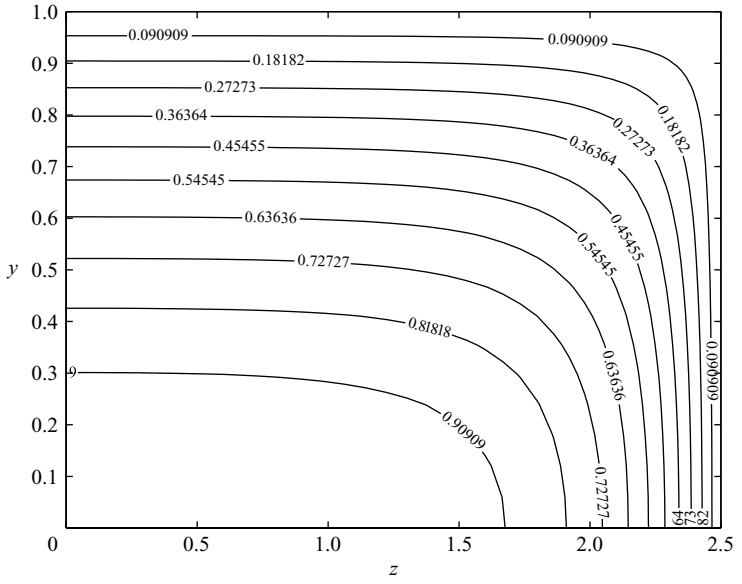


FIGURE 2. The distribution of the streamwise velocity $\bar{u}$ over the upper right-hand quarter of the duct.

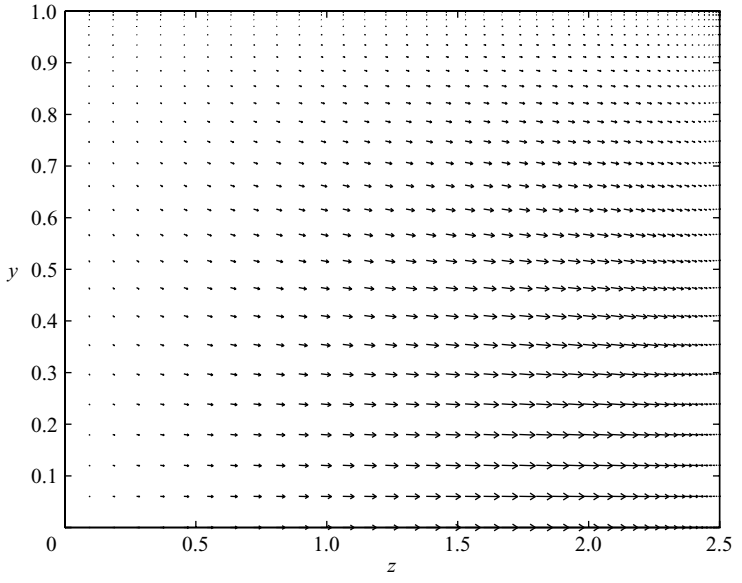


FIGURE 3. The distribution of the crossflow velocity components $\bar{v}$, $\bar{w}$ over the upper left-hand quarter of the duct.

4. Results

4.1. *Mean flow*

The mean flow at each station was computed initially with the calculation of the streamwise velocity component which, as was shown, decouples from the crossflow velocity components and is given by equation (18). Then the right-hand side of the system of equations (20) can be calculated and the aforementioned system solved together with the Laplace equation $\nabla^2\theta = 0$. The results for the case $A = 2.5$ are

https://doi.org/10.1017/S0022112006008664 Published online by Cambridge University Press

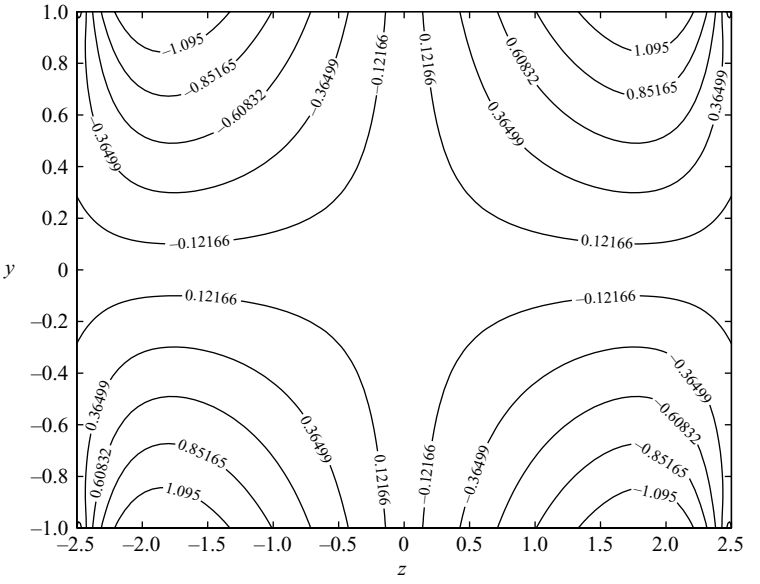


FIGURE 4. The distribution of the vorticity θ.

illustrated in figures 2–4. In figure 2, the streamwise velocity component is shown over the upper-right-hand quarter of the domain, after being normalized so that its maximum value (at the centre of the duct) is unity. Because of symmetry, the distribution of $\bar{u}(y, z)$ is the same in the other quarters of the domain. It can be observed that the effects of the sidewall become important only in a region close to them of width equal to the height of the duct, whereas close to the vertical centreline, $\bar{u}$ attains the same form with the Poiseuille flow. This becomes more apparent at larger values of the aspect ratio, as numerical results have indicated.

Furthermore, in figure 3, the crossflow velocity components are indicated over the upper-left-hand part of the duct. It can be seen that the velocity component along the largest dimension of the duct, in this case $\bar{w}$, is much larger than the other. Furthermore, it attains its highest values in a region close to the sidewalls and along the horizontal centreline, and in the vicinity of the sidewall it diminishes rapidly. In contrast, the crossflow is minimal in the vicinity of the normal centreline, agreeing with the observation above that the flow in this region resembles Poiseuille flow. It should be pointed out here that the overall magnitude of the crossflow velocity components is ϵ times smaller than $\bar{u}$, as explained in § 2.

Moreover, figure 4 illustrates the vorticity distribution over the whole domain. It is evident that the maximum vorticity is localized mainly close to the walls which are along the largest dimension, the upper and lower walls in the present case. There is also a small structure next to the remaining walls and close to the corners, but the maximum strength of the latter is much less than that of the former. Owing to the symmetry of the duct, the vorticity is characterized by antisymmetry and along both the centrelines, θ is zero.

Finally, note that the equations that yield the velocity components are independent of the Reynolds number, which means that flows with different Reynolds numbers have (non-dimensionalized) velocity components of the same distribution and magnitude. This is in contrast to external flows where, with increasing Reynolds number, the boundary layer reduces in thickness.

https://doi.org/10.1017/S0022112006008664 Published online by Cambridge University Press

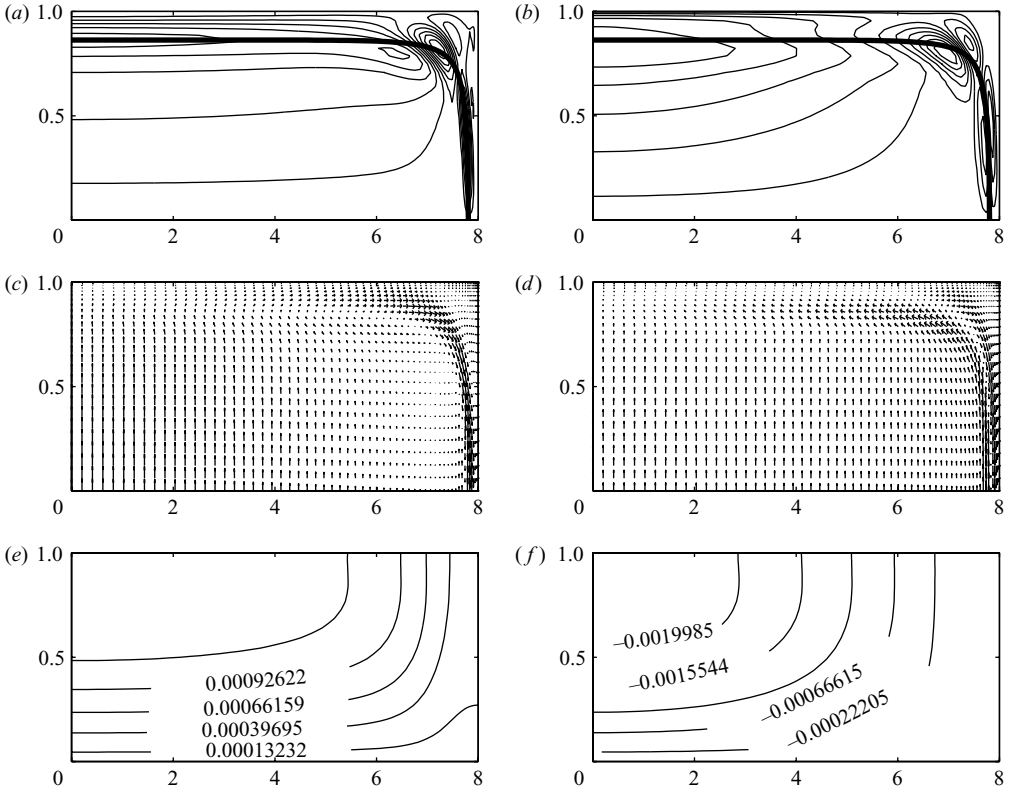


FIGURE 5. Plots for mode I in the upper right-hand quarter of the domain. (a, b) Contour plots of the real and imaginary parts of the streamwise velocity disturbance together with the critical layer $\bar{u} = \omega/\mathrm{Im}\{a\}$ (thick black line). (c, d) Vector plots of the real and imaginary parts of the velocity disturbances over a cross-section. (e, f) Contour plots of the real and imaginary parts of the pressure disturbance. (Neutral disturbance, $A = 8$, figure not to scale.)

4.2. *Instability results*

As far as the instability of the duct flow is concerned, we have carried out a series of calculations that provide the neutral curves of the non-parallel flow (diverging duct) for various Reynolds numbers and we have compared them to the corresponding ones for the parallel flow (constant aperture duct). It should be mentioned that the parallel flow calculations indicated that the most unstable of the modes is the first one, according to its characteristics as these are defined in (29). Therefore, we have concentrated on the first mode only, whose structure for the neutral case at $A = 8$ is illustrated in figure 5. It must be pointed out that the plots are not to scale in order to improve clarity. The imaginary part of the eigenvalue that corresponds to this disturbance is $\mathrm{Im}\{a\} \approx 0.9802$ and since the frequency of the neutral disturbance is found to be $\omega \approx 0.2497$, the critical layer in which $\bar{u} = \omega/\mathrm{Im}\{a\}$ lies along the contour of the $\bar{u}$-distribution where $\bar{u} \approx 0.2547$. This contour is shown in the two upper contour plots in figure 5. It is evident that the disturbance is localized in the vicinity of this critical layer.

The results of Tatsumi & Yoshimura (1990) can be used in order to predict the shape of these neutral curves. Indeed, their results are derived by solving the temporal instability problem along a duct of arbitrary but constant aspect ratio

https://doi.org/10.1017/S0022112006008664 Published online by Cambridge University Press

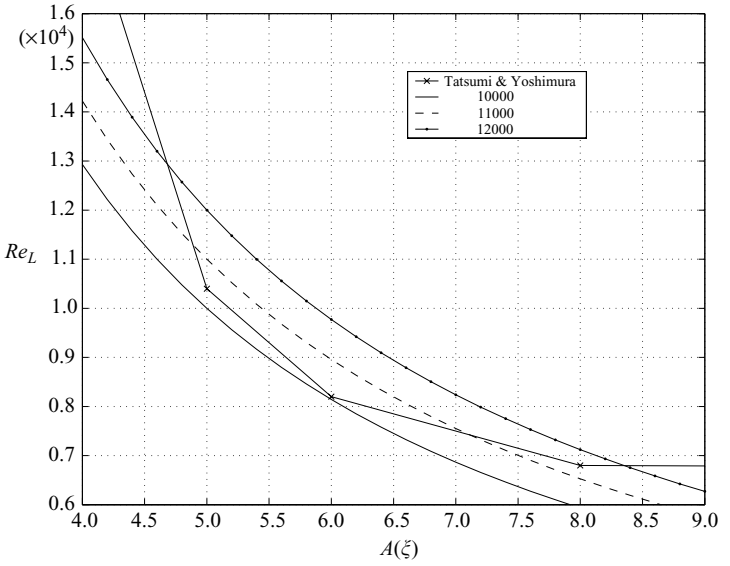


FIGURE 6. Comparison of the variation of the 'local' Reynolds number Re_L versus the aspect ratio $A(\xi)$ for various Reynolds numbers Re with the critical Reynolds numbers calculated in Tatsumi & Yoshimura (1990) for various aspect ratios.

with the streamwise velocity, the only non-zero component, normalized such that its maximum value is unity. In the present formulation, the streamwise velocity component changes along the streamwise direction. However, it is possible to re-normalize the equations so that $\bar{u}(\xi) = 1 = \text{const}$ and the Reynolds number, Re and frequency ω vary along ξ. In this case we have:

$$Re_L(\xi) = \kappa_0 Re/I(\xi),$$

where Re is the Reynolds number of the original formulation and Re_L a 'local' Reynolds number of the modified formulation. If we choose κ_0 such that $\bar{u}(\xi = 5) = 1 \Rightarrow Re_L(\xi = 5) = Re$, we can plot the 'local' Reynolds number versus the aspect ratio $A(\xi)$. In the same figure we can plot the results of Tatsumi & Yoshimura (1990) for the critical Reynolds number of the first mode for various aspect ratios. This is illustrated in figure 6 for $Re = 10\,000, 11\,000$ and $12\,000$. We can see that, for the two larger Reynold numbers, there is a finite region of aspect ratios, and therefore of streamwise positions ξ, along which the 'local' Reynolds number is larger than the critical ones given by Tatsumi & Yoshimura (1990). For the smaller Reynolds number, the curve corresponding to Re_L does not cross the critical Reynolds number line. Therefore, it appears that the flow for which $Re = 10000$ and $\bar{u}(\xi = 5) = 1$ is stable. Finally, it is obvious that there will always be a finite region of instability, irrespective of how large the Reynolds number Re is. This means that the neutral curves are closed.

We used a Newton iteration method in order to find the position of the neutral points with tolerance for the absolute value of the growth rate equal to 10^{-8} for the cases $Re = 10\,200, 11\,000$ and $12\,000$. The last two values render the two closed curves illustrated in figure 7, whilst the first one corresponds to the case in which the flow becomes neutrally stable at a single ξ-position and remains stable elsewhere. However, these results correspond to the case when the flow is considered to be

https://doi.org/10.1017/S0022112006008664 Published online by Cambridge University Press

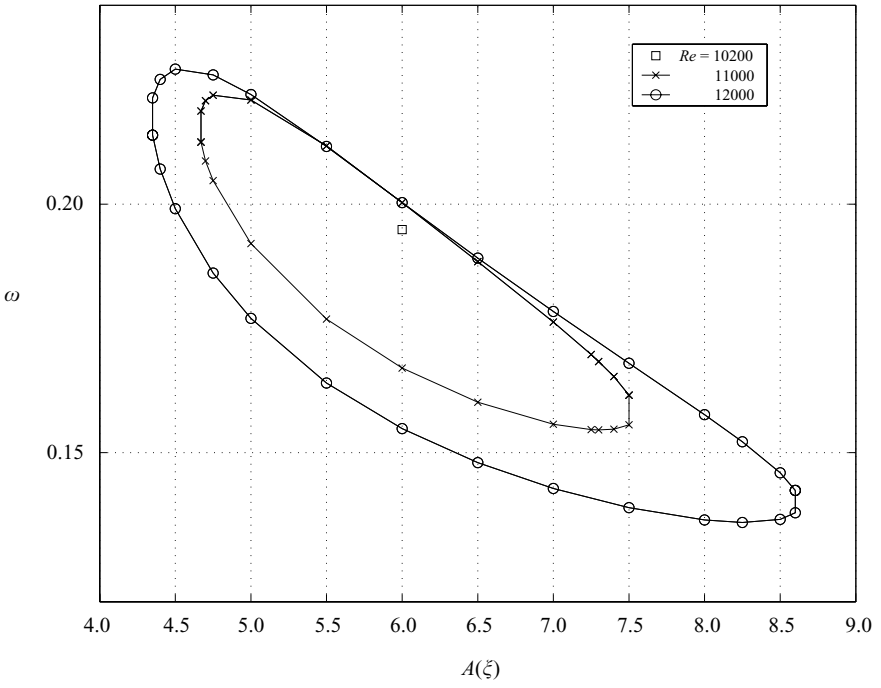


FIGURE 7. The neutral curves based on the zeroth-order approximation of the growth rate for three different Reynolds numbers.

locally parallel. Of course this is in direct contrast to the diverging nature of the tube, which led us in the first place to the definition of the 'global' and 'local' Reynolds numbers. Therefore, the aforementioned results may not be used in order to draw any conclusions for the regions of instability of the flow under consideration.

The non-parallel character of the flow can be included in the calculation of the position of the neutral curves by use of the correction (32). The corrected neutral curves for the cases $Re = 11\,000$ and $Re = 12\,000$ are illustrated in figure 8. The corrections were calculated after setting $\epsilon = 0.001$, $\epsilon = 0.005$ and $\epsilon = 0.015$. Note here that the range of validity of the expansion procedure is much smaller near the top left-hand and bottom right-hand parts of the neutral curve. This is because the horizontal and vertical tangents to the neutral curve with $\epsilon = 0$ occur close to each other so that even very small values of ϵ produce large shifts in the neutral curve. This means that the 'wiggles' in the neutral curves in the top left-hand corner are artefacts of our using the asymptotic theory in a place where it is not valid.

5. Conclusions

It was demonstrated above that the non-parallel effects lead to a destabilization of the flow, both for the lower and upper branch neutral solutions corresponding to the parallel-flow approximation. Furthermore, it appears that the correction to the parallel-flow solution is larger for the smaller Reynolds numbers. This should be expected, since the smaller the Reynolds number becomes, the closer the critical layer lies to the centre of the duct. In turn, this means that the flow is affected more in the small Reynolds numbers, even with the same rate of change of the aspect ratio.

https://doi.org/10.1017/S0022112006008664 Published online by Cambridge University Press

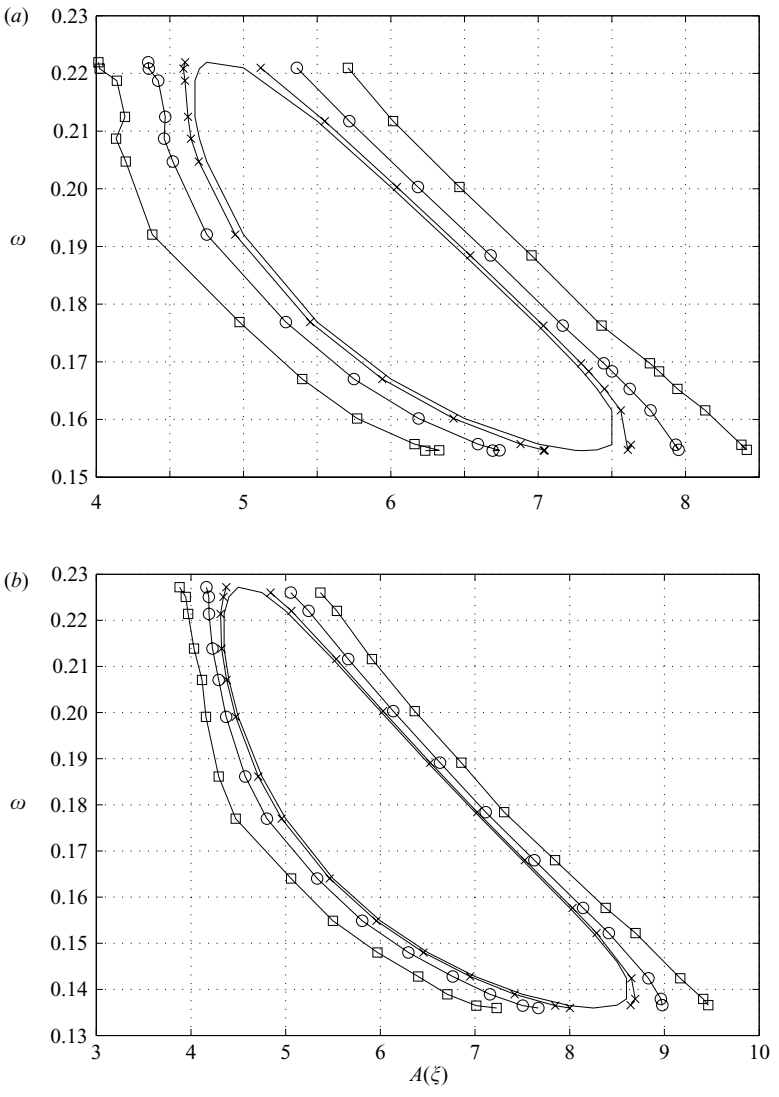


FIGURE 8. Combination of the neutral curves based on the zeroth- and first-order approximations of the growth rate for (*a*) $Re = 11\,000$ and (*b*) $Re = 12\,000$. (—, parallel flow $\epsilon = 0$; ⊣⊢, $\epsilon = 0.001$; ⊖, $\epsilon = 0.005$; □, $\epsilon = 0.015$.)

Although the results that were shown here refer to the $\bar{u}(\xi = 5) = 1$ case, they can be used as an indication of the shape of the neutral curves for other cases, since the former value is linked to the normalization of the velocity that leads to the non-dimensional Navier–Stokes equations. Therefore, with a different reference velocity u^*_{ref}, the $\bar{u} = 1$ position can be transferred anywhere in the ξ-direction and after the corresponding change of the Reynolds number $Re = u^*_{ref} L^*/\nu^*$ and frequency $\omega = \omega^* L^*/u^*_{ref}$ the position of the parallel-flow approximation neutral curves can be guessed. The related non-parallel flow neutral curves should follow the shape of the parallel-flow ones, as was shown in the treated cases.

Furthermore it was shown in Tatsumi & Yoshimura (1990) that there is a critical aspect ratio below which all disturbances are damped, namely $A_c = 3.2$. This is a

https://doi.org/10.1017/S0022112006008664 Published online by Cambridge University Press

parallel-flow stability result. In general, the neutral curve corresponding to the non-parallel flow under the same conditions could be different from the parallel-flow one so that stable conditions under the parallel-flow approximation become unstable under the non-parallel flow approximation. However, since the critical point is neutral for Reynolds number equal to infinity, and taking into account the above observation that for increasing Reynolds numbers the changes due to the non-parallel character of the flow become less important, we conclude that $A = 3.2$ yields the value of the critical aspect ratio below which no unstable disturbance can exist also for the non-parallel flow.

Unfortunately, the existing experimental results refer to the case of a constant-aperture duct with a large aspect ratio ($A > 8$). Therefore, they cannot be used for the verification of the present theoretical results. Measurements of the disturbance quantities under controlled conditions and with the introduction of well-defined disturbances are essential in order to be able to make any comparisons. In the light of the existing experimental results and their comparison with previous theoretical works of Tatsumi & Yoshimura (1990), it becomes evident that full agreement between theoretical and experimental results cannot be achieved owing to the nonlinearities existing in the experiments. In the present problem, this will become even harder because of the diverging character of the duct and the sensitivity of the flow even to slight changes of the pressure gradient.

REFERENCES

Davis, S. J. & White, C. M. 1928 An Experimental Study of the Flow of Water in Pipes of Rectangular Section. *Proc. R. Soc. Lond.* A, **119**, 92–107.

Galionis, I. 2003 On the linear instability of spatially varying incompressible flows. PHD thesis, Imperial College.

Gaster, M. 1974 On the effects of boundary-layer growth on flow stability. *J. Fluid Mech.* **66**, 465–480.

Hall, P. 1983 The linear development of Görtler vortices in growing boundary layers. *J. Fluid Mech.* **130**, 41–58.

Hocking, L. M. 1978 Nonlinear instability of flow in a rectangular pipe with large aspect ratio. *Z. Angew. Math. Phys.* **29**, 100–111.

Kao, T. W. & Park, C. 1970 Experimental investigations of the stability of channel flows. Part 1. Flow of a single liquid in a rectangular channel. *J. Fluid Mech.* **43**, 145–164.

Rosenhead, L. M. 1963 *Laminar Boundary Layers.* Oxford University Press.

Saad, Y. 1992 *Numerical Methods for Large Eigenvalue Problems.* Halsted.

Schiller, L. 1923 Über den Strömungswiderstand von Rohren verschiedenen Querschnitts und Rauhigkeitsgrades. *Z. Angew. Math. Mech.* **3**, 2–13.

Tatsumi, T. & Yoshimura, T. 1990 Stability of the laminar flow in a rectangular duct. *J. Fluid Mech.* **212**, 437–449.

Theofilis, V., Duck, P. W. & Owen, J. 2004 Viscous linear stability analysis of rectangular duct and cavity flows. *J. Fluid Mech.* **505**, 249–286.

https://doi.org/10.1017/S0022112006008664 Published online by Cambridge University Press